International Journal for Uncertainty Quantification, 3 (6): 523–540 (2013)

EFFECT OF PARAMETRIC UNCERTAINTIES ON THE EFFECTIVENESS OF DISCRETE PIEZOELECTRIC SPATIAL MODAL FILTERS

Marcelo A. Trindade, [*] ***Carlos C. Pagani, Jr., Leopoldo P. R. Oliveira, & Ernesto Massaroppi, Jr.***

Department of Mechanical Engineering, Sao Carlos School of Engineering, University of Sao Paulo, Av. Trabalhador Sao-Carlense, 400, Sao Carlos-SP, 13566-590, Brazil

Original Manuscript Submitted: 4/30/2012; Final Draft Received: 9/30/2012

Modal filters may be obtained by a weighted sum of the signals of an array of sensors distributed on the host structure. However, the effect of parametric uncertainties on the effectiveness of the modal filter has received little attention. This work presents some numerical and experimental results on the effect of uncertainties of sensor array spatial distribution and weighting coefficients on the modal filtering effectiveness. For that, a free rectangular plate with twelve bonded piezoelectric sensors is considered. The spatial distribution of the array of piezoelectric sensors was optimized in a previous work to improve the effectiveness and frequency range of a set of modal filters. An experimental implementation of the modal filters was performed through a voltage divider and summing amplifier circuits and used to validate the performance of the modal filters. From numerical and experimental analysis, it was noticed, however, that the effectiveness of the modal filters are quite sensitive to the array spatial distribution and weighting coefficients. First, the effect of uncertainties of the array spatial distribution on the output of the modal filters was analyzed numerically using a finite element model. In this case, the main challenge was the cost of function evaluation and, thus, focus was put on solutions for the parameters sampling and approximations using response surface methods. Then, the effect of uncertainties of the weighting coefficients was evaluated using stochastic modeling combined with the measurement of individual responses of piezoelectric sensors. Confidence intervals for the modal filters output were evaluated and compared to experimental results with satisfactory results.

KEY WORDS: *modal filters, piezoelectric sensors, parametric uncertainties, positioning optimization*

1. INTRODUCTION

Piezoelectric materials have been extensively used to build integrated sensors and actuators shaped as small, thin, and lightweight patches of several geometries that can be bonded to or embedded in flexible structures. They are relatively inexpensive and present the necessary electromechanical coupling to provide satisfactory sensing and actuating effectiveness for very flexible structures in bending [1]. Integrated piezoelectric patches have been applied to several applications, such as active and passive vibration control [2, 3], damage detection and structural health monitoring [4, 5], and power/energy harvesting from mechanical vibrations [6].

When integrated into a vibrating flexible structure, surface-bonded or embedded piezoelectric patches provide adequate electromechanical coupling to low-frequency vibration modes and, thus, may be used to monitor and/or control them. For certain applications, it would be interesting to control only a small subset of the structural vibration modes. In these cases, the concept of modal sensors and actuators could be used to improve the overall performance of the control system [7, 8]. In general terms, the idea of controlling only a selection of vibration modes aims (i) at minimizing the required control effort, since no (or less) energy would be spilled with untargeted vibration modes,

[*]Correspond to Marcelo A. Trindade, E-mail: trindade@sc.usp.br, URL: http://www.eesc.usp.br/labdin

2152–5080/13/$35.00

and (ii) at reducing spillover and instabilities issues of active controllers, since excitation of untargeted and unmodeled vibration modes would be diminished. The development of active control strategies with optimal performance using modal sensors and actuators has been the object of intensive research [9–13]. The performance of modal controllers depends on several parameters. The size, form, and effective electromechanical coupling coefficient of a piezoelectric material must be considered in the development of modal sensors and actuators. Although pioneer works have proposed continuous modal sensors and actuators [8], the evolution of modal filter techniques and its applications to active vibration control indicates several advantages in the use of an array of discrete sensors instead.

Continuous modal sensors are designed to ensure shape coupling between sensing material and elastic strain due to the target vibration modes of the host structure [8, 11]. An array of sensors, on the other hand, is in general composed by small piezoceramic patches and depends on a convenient weighted sum of sensors' signals to achieve a modal filtered output signal [9, 10]. Several methodologies have been used for the evaluation of the weighting coefficients for signals measured by an array of sensors. They can be divided into three groups: target modes output match, optimization techniques, and frequency response function (FRF) matrix inversion. Whenever the target mode shapes are known/predicted and their reading in terms of output amplitude in each sensor of the array can be identified, a technique, proposed by Meirovitch and Baruh [7] and based on the orthogonality of normal modes, considers that the weighting coefficients should match the output of each sensor for the target mode. This technique may be strongly affected by spatial aliasing. The weighting coefficients may also be evaluated using an optimization algorithm to minimize the difference between the weighted response and a desired modal response. Shelley [14] proposed an online adaptation algorithm to estimate the desired modal response and update the weighting coefficients. The third group of methods is based on the inversion of the FRF matrix, which can be either predicted by a numerical model [12] or experimentally measured [14], in order to shape the target filtered response.

These techniques may lead to high-performance modal filters, but generally within a limited frequency range. Preumont et al. [10] have suggested that the frequency range of high-performance filtering depends on the relation between the number of vibration modes to be filtered, in that frequency range, and the number of sensors in the array. They concluded that the number of sensors in the array should be larger than the number of vibration modes to be filtered. Although this is true for an arbitrarily distributed array of sensors, it is possible to show that the location of the sensors, that is, the array spatial distribution, has a significant effect on the observability of the vibration modes and, thus, on the filtering performance of modal filters derived from it. Previous works [15] have indicated that it is possible to increase the number of vibration modes filtered by a modal filter, and thus the frequency range, using a fixed number of sensors provided the spatial distribution of the sensors array is optimized. It has been shown that the effective frequency range can be enlarged by 25%–50%. However, this optimization may also lead to a higher sensitivity of modal filters performance on sensors positioning. Weighted-sum discrete modal filters may also be sensitive to a proper tuning of the weighting coefficients.

Therefore, this work presents a robustness analysis of modal filters using a spatial distribution optimized array design with a reduced number of sensors subjected to uncertainties in the weighting coefficients and sensors positioning. For the weighting coefficients uncertainties, this is done using stochastic modeling tools to build a probabilistic model of the uncertain parameters and the Monte Carlo method to evaluate the realizations of modal filters performance indices using experimental measurements from the piezoelectric sensors. For the sensors positioning uncertainties, a sampling-based sensitivity analysis is performed. The Latin hypercube sampling technique is used to reduce the number of samples and alleviate the computational cost of analyzing multiple array spatial distributions. In addition, another strategy using response surface methods is considered to improve the number of samples and to provide approximations for smaller positioning uncertainties.

2. DESIGN OF MODAL FILTERS

The design of a modal filter from an array of sensors requires the output signals of each sensor to be weighted and summed such that (i) the responses of the target vibration modes are maximized, and (ii) the responses of the undesired vibration modes are minimized. Therefore, it is possible to consider the FRF of an equivalent single degree of freedom system with natural frequency ω_i and damping factor ζ_i, corresponding to the target ith vibration mode, as the desired FRF of the weighted signal of the modal filter, which can be written as

$$g_i(\omega) = \frac{2\zeta_i \omega_i^2}{\omega_i^2 - \omega^2 + 2j\zeta_i \omega_i \omega}. \tag{1}$$

Whenever the vibration modes are weakly damped and relatively well spaced, the resonance peaks are well defined and, thus, (1) represents a realistic objective for the filtered FRF signal. Let $\mathbf{Y}$ be a matrix with columns that represent the FRFs of the n selected sensors in the array and discretized in a frequency domain $[\omega_1, \ldots, \omega_m]$. Let $\mathbf{G}_i = [g_i(\omega_1), \ldots, g_i(\omega_m)]$ be the vector representing (1) in the discrete frequency domain. The vector of coefficients α_i which equates the filtered output (weighted sum of sensors outputs) to the one defined by $\mathbf{G}_i$ is the solution of

$$\begin{bmatrix} Y_1(\omega_1) & \cdots & Y_n(\omega_1) \\ \vdots & \ddots & \vdots \\ Y_1(\omega_m) & \cdots & Y_n(\omega_m) \end{bmatrix} \begin{bmatrix} \alpha_{i1} \\ \vdots \\ \alpha_{in} \end{bmatrix} = \begin{bmatrix} g_i(\omega_1) \\ \vdots \\ g_i(\omega_m) \end{bmatrix}. \tag{2}$$

In general, the linear system defined by (2) admits only approximate solutions, which will be denoted $\alpha_i^\dagger$. The vector of weighting coefficients $\alpha_i^\dagger$ represents the best solution, in a least squares-sense, for the design of a modal filter which isolates the ith vibration mode response. If several vibration modes are to be considered simultaneously as target modes for the filter design, it is necessary to define $\mathbf{G}$ as the matrix of target FRFs with dimension $m \times p$, where p denotes the number of target modes. Consequently, the approximate solution of (2), $\alpha^\dagger$, is a matrix of dimension $n \times p$, that is one column vector of weighting coefficients for each one of the target modes. This may be written in a compact form as

$$\mathbf{Y}\alpha^\dagger = \mathbf{G}. \tag{3}$$

Actually, $\mathbf{Y}\alpha^\dagger$ approximates $\mathbf{G}^\dagger$, a matrix with columns that are the orthogonal projection of the columns of $\mathbf{G}$ onto the space spanned by the columns of $\mathbf{Y}$. The traditional Moore-Penrose pseudo-inverse solution of (3) for a full column rank $\mathbf{Y}$ matrix (with columns that are linearly independent) may be obtained by pre-multiplying (3) by $\mathbf{Y}^{\mathrm{H}}$, the Hermitian of $\mathbf{Y}$, such that

$$\mathbf{Y}^{\mathrm{H}}\mathbf{Y}\alpha^\dagger = \mathbf{Y}^{\mathrm{H}}\mathbf{G}, \text{ such that } \alpha^\dagger = \left(\mathbf{Y}^{\mathrm{H}}\mathbf{Y}\right)^{-1}\mathbf{Y}^{\mathrm{H}}\mathbf{G}. \tag{4}$$

On the other hand, for a full column rank matrix, the inversion of $\mathbf{Y}^{\mathrm{H}}\mathbf{Y}$ is unnecessary and computationally inefficient, since $\mathbf{Y}$ may be decomposed through QR decomposition, where $\mathbf{Q}$ is an orthonormal matrix and $\mathbf{R}$ is upper triangular, such that $\mathbf{Y} = \mathbf{QR}$ and (4) can be rewritten, after expansion and accounting for $\mathbf{Q}^{\mathrm{H}}\mathbf{Q} = \mathbf{I}$, as

$$\alpha^\dagger = \mathbf{R}^{-1}\mathbf{Q}^{\mathrm{H}}\mathbf{G}. \tag{5}$$

Notice that the inverse of $\mathbf{R}$ does not need to be evaluated; instead the upper triangular linear system, $\mathbf{R}\alpha^\dagger = \mathbf{Q}^{\mathrm{H}}\mathbf{G}$, is solved through back substitution, which is computationally more efficient. For all the cases studied in the present work, the solution through QR decomposition was always convenient, since the FRF matrix has had full column rank. If at least two columns of the FRF matrix are linearly dependent, the singular value decomposition (SVD) is the suitable method to approximate the least-squares solution. In practice, the truncation of matrix $\mathbf{Y}$ over a given frequency range will affect its QR decomposition and, thus, the approximate solution of the linear system (3). Recent works have shown that there is a value for truncation frequency such that all vibration modes inside a given frequency range are perfectly filtered, except the target ones, whereas resonances larger than the truncation frequency are not filtered [10].

3. PREDICTED PERFORMANCE OF OPTIMAL SPATIAL MODAL FILTERS

In a previous work, the modal filter design technique presented in the previous section was applied to a plate with bonded piezoceramic patches acting as sensors [15]. A free rectangular aluminum plate, of dimensions 320×280×3 mm, was considered as the host vibrating structure. A transversal point force applied near the upper-right corner of the plate was considered for the evaluation of frequency response functions in all cases. The study aimed at finding a spatial distribution of twelve piezoceramic patches to optimize the performance of two modal filters, designed to

isolate the first and second vibration modes up to 1000 Hz. Using a genetic algorithm optimization strategy, the twelve piezoceramic patches were chosen between a regular array of 36 identical thickness-poled piezoceramic patches, with dimensions $25\times25\times0.5$ mm, bonded to the upper surface of the plate. More details can be found in [15].

Figure 1 presents the normalized filter output, such that the amplitude at target resonances is unitary, and the corresponding optimal spatial distribution, in which the 12 selected sensors are highlighted from the original array of 36 sensors. The spatial distribution was optimized so that two selected modal filters, one designed to isolate the first vibration mode and the other designed to isolate the second vibration mode, could be effective up to 1000 Hz. Figure 1 shows that effective filtering could be obtained up to 1100 Hz (with unfiltered noise below 1% of the resonant response). This means that four additional resonances could be filtered compared to an arbitrary spatial distribution of 12 sensors. For an arbitrary FRF matrix $\mathbf{Y}$, (5) may yield complex weighting coefficients vectors α_j. Since, in practice, it could be much more difficult to implement complex weighting coefficients to the FRF measured by each sensor, the response of the corresponding modal filters evaluated using only the real part of vectors α_j were also considered. Figure 1 shows that the modal filters' outputs are not significantly altered by neglecting the imaginary part of the weighting coefficients. This indicates that a simple voltage divider circuit (potentiometer) could serve as an analogic weighting of the sensors' outputs.

4. ANALYSIS OF POSITIONING UNCERTAINTIES

This section presents an analysis of the effect of random uncertainties on the positioning of the twelve sensors of the optimal spatial distribution presented previously. As discussed previously, spatial distribution optimization allows as to use fewer sensors than would be necessary otherwise for the design of modal filters. However, modal filters based on such optimal arrays of sensors become sensitive to the positioning of the sensors. Therefore, it is important to quantify the sensitiveness of a given optimal spatial distribution to perturbations on the positioning of its sensors. Instead of using local methods, such as gradient-based methods, to perform a sensitivity analysis, here a sampling-based analysis is used [16]. This may be quite difficult since, for each perturbation in a given sensor positioning, the dynamic stiffness of the structure is modified and, thus, a new structural model should be constructed and used to evaluate the voltage frequency responses of all sensors in the array. This fact not only leads to higher computational cost, due to multiple evaluations of the structural harmonic response, but also requires special attention to whether the changes in output are due to perturbations in sensor positioning or to the reconstruction of the structural model.

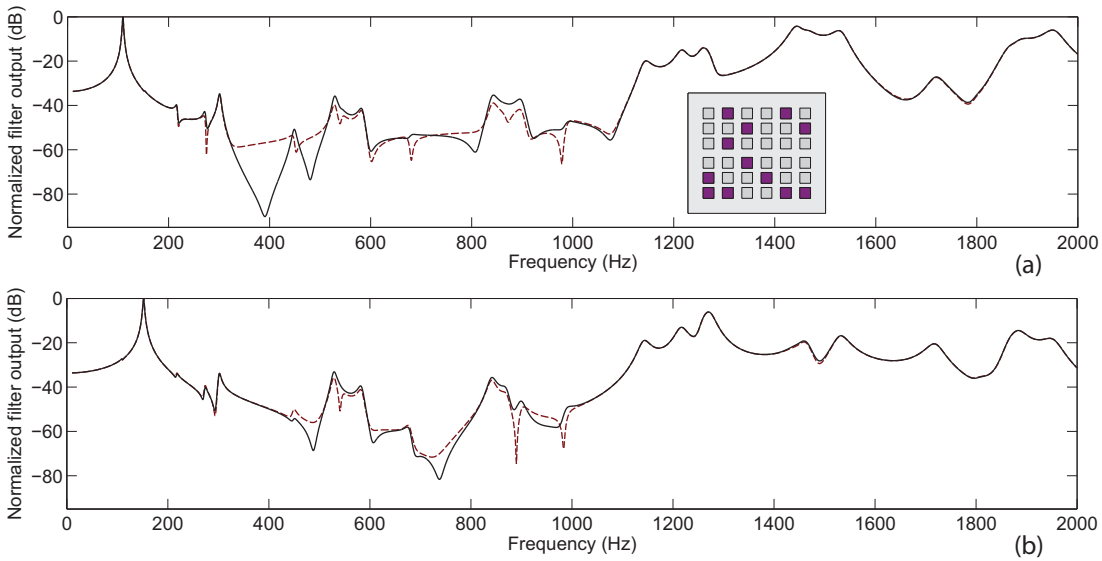

FIG. 1: Normalized outputs of first (a) and second (b) modal filters using complex (dashed) and real (solid) weighting coefficients.

The methodology used in this work to prevent variability due to structural modeling was to consider a fixed finite element mesh over which the piezoelectric sensors can be repositioned. Two finite element models were built with mesh refinements of 5 and 2.5 mm and thus allow positioning perturbations in steps of 5 and 2.5 mm, respectively. In the case of the finer mesh, 14336 (128×112) SHELL99 elements were used for the plate, while 200 SOLID226 elements were considered for each piezoceramic patch. To ensure a perfect bonding between piezoceramic patches and plate, the nodes on the bottom surface of the patches were coupled to the ones on the top surface of the plate. To this end, the nodes of the SHELL99 elements were offset to the contact surface with the SOLID226 elements. It is unnecessary to state that the finer mesh increases heavily the computational cost of one harmonic analysis in ANSYS, as compared to a coarser mesh model. A transversal point force applied near the upper-right corner of the plate (with position independent of mesh refinement) is considered for the evaluation of frequency response functions in all cases. Figure 2 shows the optimal spatial distribution together with the finite element mesh considered and three of the one hundred perturbed spatial distributions used in the present analysis.

4.1 Uncertainty Quantification Using LHS

As a first strategy for the uncertainty quantification, 100 random perturbed spatial distributions were obtained using Latin hypercube sampling (LHS), which is an interesting method when the number of samples is relatively small and consists of maximizing the distance between the samples. Since the positioning perturbation must be performed in steps of 2.5 mm, two vectors of normalized displacements in x and y directions relative to the optimal position, $\Delta\bar{x} \in \{-1, 0, 1\}$ and $\Delta\bar{y} \in \{-1, 0, 1\}$, were constructed for each piezoelectric sensor. This leads to a vector of 24 elements with values in $\{-1, 0, 1\}$ defining the perturbed spatial distribution described by the displacements along x and y directions of each piezoelectric sensor relative to its optimal position ($\Delta x = 2.5\Delta\bar{x}$ mm and $\Delta y = 2.5\Delta\bar{y}$ mm). Then, the LHS technique was used to construct 100 samples of the 24-elements vector.

For each perturbed spatial distribution, the FRF was evaluated for each one of the 12 piezoelectric sensors and, then, used to evaluate the modal filters output responses through multiplication by the real part of the optimal (unperturbed) vector of weighting coefficients, $\bar{\alpha}$. The results for the first and second modes modal filters output are shown in Fig. 3 for all perturbed spatial distributions. A large variation of the filter output response can be noted inside the frequency range of interest in which the response should be filtered.

To save computational effort, the same analysis was performed for higher (5-mm) displacement steps using the finite element model with coarser mesh (5-mm mesh refinement). The results are presented in Fig. 4. Although not presented here, a comparison between the unperturbed responses using the 2.5-mm and 5-mm spaced meshes was made and found to have no significant effect on the evaluation of the modal filters output responses. Therefore, the unperturbed response using the finer mesh (2.5 mm) can be used as reference to the perturbed responses with 5-mm displacement steps.

Then, two methodologies were considered to quantify the filtering quality decrease due to the spatial distribution perturbations. First, the realizations of filter output amplitudes, for each frequency point, were used to evaluate the mean values and the 95% confidence interval of the realizations, using the 2.5% and 97.5% percentiles.

The results for both first and second modes modal filters and for smaller (2.5-mm) and larger (5-mm) displacement steps are presented in Fig. 5. It can be noticed that the responses differ mainly inside the frequency range of interest. As expected, smaller values for the perturbation (displacement) steps lead to better filtering quality. It can also be

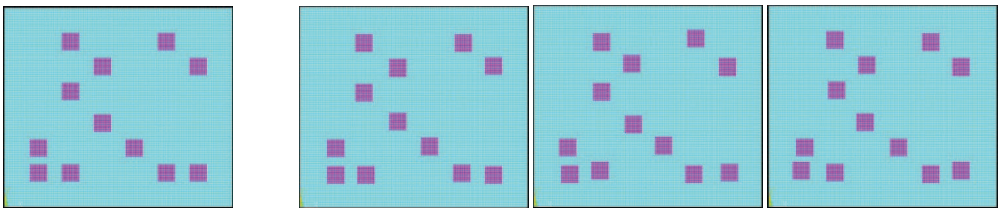

FIG. 2: Optimal spatial distribution for the isolation of the first two vibration modes and three of its arbitrary perturbations.

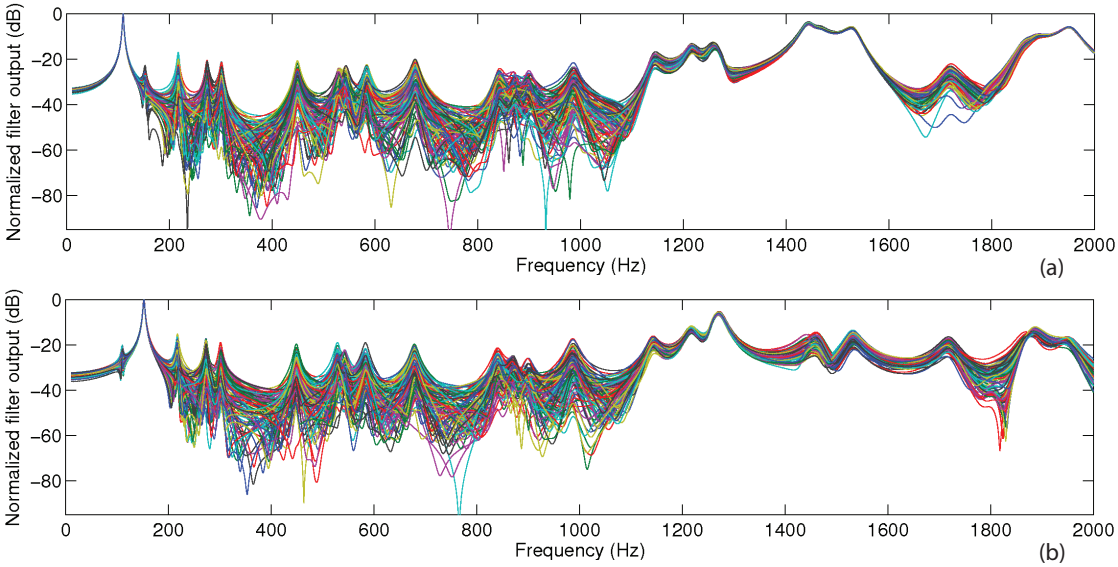

FIG. 3: Normalized outputs for first (a) and second (b) modal filters using perturbed spatial distributions with 2.5-mm displacement steps.

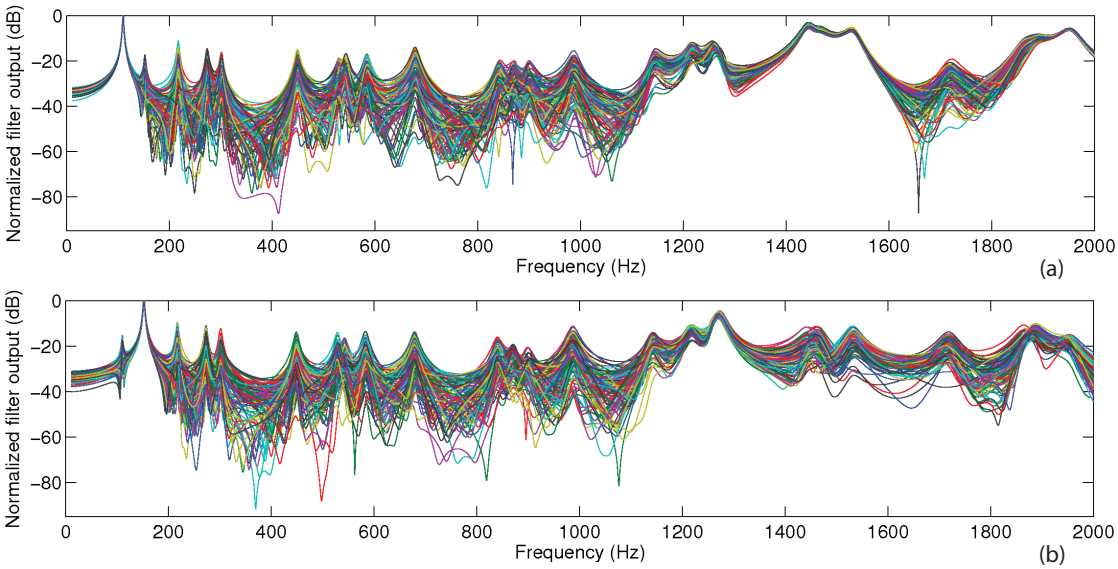

FIG. 4: Normalized outputs for first (a) and second (b) modal filters using perturbed spatial distributions with 5-mm displacement steps.

observed that the perturbation yields a mean output for which the amplitude of the filtered ressonances are set to the same order of magnitude. This suggests that the perturbation decreases the filtering quality more for the resonances that are better filtered.

From the 95% confidence interval, the maximum error for the first mode modal filter is approximately 21%, for a 5-mm perturbation, and 11%, for a 2.5-mm perturbation (Fig. 5). For the second mode modal filter, these maximum errors are, respectively, 26% and 13%. The maximum error is located at the third resonance for all cases. Although it

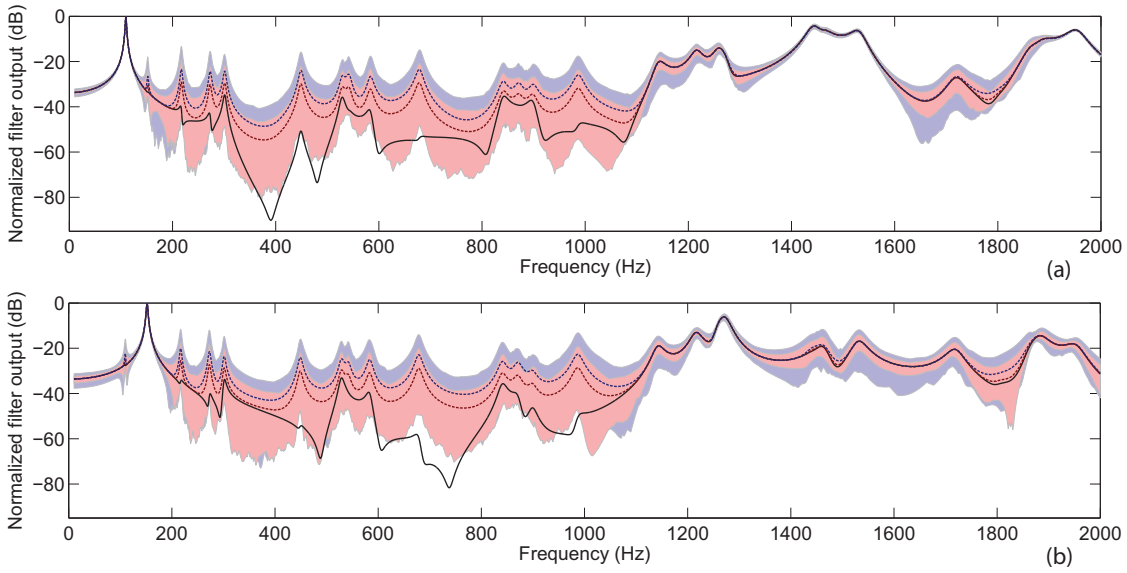

FIG. 5: Mean and 95% confidence interval (percentiles) of the normalized first (a) and second (b) modes filter outputs compared to the unperturbed (black) output for 2.5-mm (red) and 5-mm (blue) displacement steps.

is not advisable to interpolate these results to estimate the confidence interval for other perturbation magnitudes, it is reasonable to guess that perturbations smaller than 2.5 mm should lead to errors smaller than 10%.

Considering the mean outputs, the maximum errors for the first and second modes modal filters are, respectively, 6.7% and 10% for larger perturbation and 3.5% and 5.5% for smaller perturbation. The average filtering errors for the first and second modes modal filters over the frequency range of interest (200–1000 Hz) are, respectively, 2% and 2.5% for larger perturbation and 1% and 1.3% for smaller perturbation.

Since there is no guarantee that the probability distribution of filter output amplitudes is well represented by the relatively small sample size considered here, a second methodology was considered to quantify the loss of filtering quality due to the spatial distribution perturbation. Figure 6 shows the limiting intervals evaluated using the minimum and maximum values for each frequency. It can be noticed that Figs. 5 and 6 are similar, apart from a less smooth lower interval and wider intervals for the latter. In terms of maximum filtering errors (Fig. 6), worst-case results are 27% (first mode) and 34% (second mode) for larger perturbation and 14% (first mode) and 17% (second mode) for smaller perturbation.

4.2 Uncertainty Quantification Using RSM

The analysis performed in the previous section is useful in providing a first estimation on how sensitive the modal filter output is to positioning perturbations. However, it has limited application since it does not account for a realistic probability distribution of the positioning uncertainties. Moreover, the cost of increasing the number of samples is too high since one modal analysis and one frequency response needs to be performed for each spatial distribution. Besides, in order to account for smaller positioning perturbations, it would be necessary to refine even further the finite element mesh which would increase even more the computational cost of the procedure.

Aiming primarily at the reduction of computational cost and better estimation of the confidence intervals of the modal filter output, a second strategy for uncertainty quantification using a response surface method (RSM) is proposed in this section. The goal of the RSM is to replace the frequency response functions evaluated using the finite element model for each perturbed array of sensors by a response surface approximation. Hence, a much smaller number of finite element calculations are needed. The main hypothesis considered in this method is that perturbations on the position of a given piezoelectric patch only affect significantly the output of this patch. Therefore, four individual

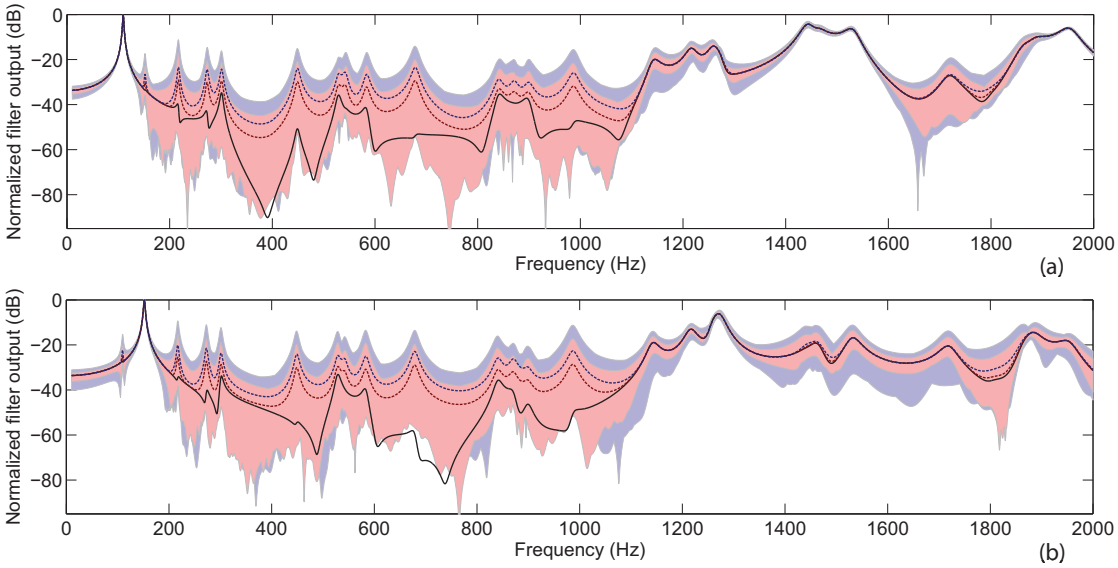

FIG. 6: Limiting intervals (minimum-maximum) of the normalized first (a) and second (b) modes filter outputs compared to the unperturbed (black) output for 2.5-mm (red) and 5-mm (blue) displacement steps.

perturbations were performed in each of the 12 piezoceramic patches, namely one mesh step (2.5 mm) to the left, right, up, and down. A schematic representation of these individual perturbations is shown in Fig. 7, where the perturbation on the position of one of the 12 patches is illustrated. Since four individual perturbations are considered for each one of the twelve patches, this leads to 48 perturbed spatial distributions.

These perturbed spatial distributions were then used to evaluate the FRF for each one of the 12 piezoelectric sensors and, then, used to evaluate the modal filters output responses through multiplication by the real part of the optimal (unperturbed) vector of weighting coefficients, $\bar{\alpha}$. The differences between the perturbed modal filters output responses and the nominal one yield the sensitivity functions $\Delta\mathbf{G}_j^+$ (for right, x^+, and up, y^+, displacements) and $\Delta\mathbf{G}_j^-$ (for left, x^-, and down, y^-, displacements). Figures 8 and 9 show the behavior of the sensitivity functions $\Delta\mathbf{G}_j^+$ and $\Delta\mathbf{G}_j^-$ (solid lines) compared to the nominal filter output (dashed line). It is noticeable that the positioning perturbations may indeed affect the filtering quality along the frequency range of interest (200–1000 Hz).

Based on the evaluated sensitivity functions, response surfaces were constructed for the first and second modal filter outputs using the following quadratic interpolation function for perturbations in x and y directions:

$$\mathbf{G}_{\text{int}} = \mathbf{G}_N + \sum_j \{[0.5\beta_j(\beta_j + 1)]\Delta\mathbf{G}_j^+ + [0.5\beta_j(\beta_j - 1)]\Delta\mathbf{G}_j^-\}, \tag{6}$$

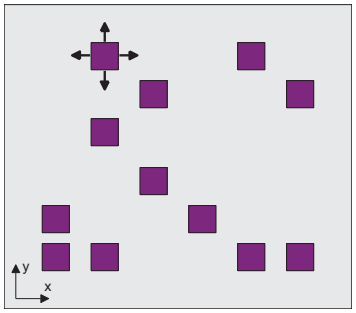

FIG. 7: Schematic representation of individual perturbations for the evaluation of the sensitivity functions.

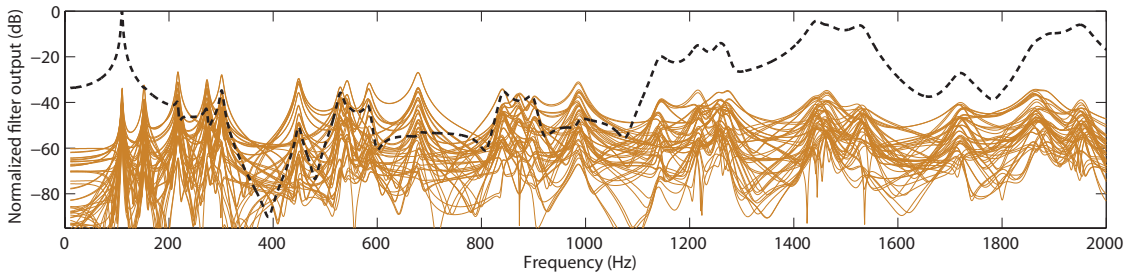

FIG. 8: Sensitivity $\Delta\mathbf{G}_j^{+/-}$ (solid) of first modal filter output to individual perturbations in patches position.

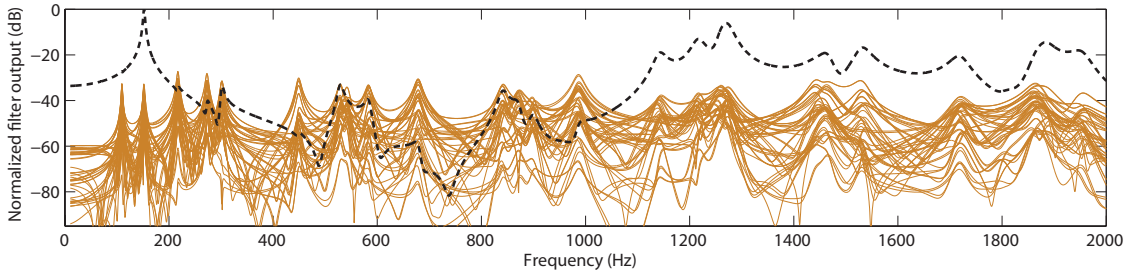

FIG. 9: Sensitivity $\Delta\mathbf{G}_j^{+/-}$ (solid) of second modal filter output to individual perturbations in patches position.

where $\mathbf{G}_N$ is the vector of nominal filter outputs for each frequency point, and $\Delta\mathbf{G}_j^{+}$ and $\Delta\mathbf{G}_j^{-}$ are, respectively, the vectors of filter output variations for positive (right or up) and negative (left or down) perturbations in patch positions for each frequency point. β_j are the normalized displacements from the nominal position; that, is $\beta_j = 1$ and $\beta_j = -1$ lead to the displacement of a patch by one mesh step in the positive and negative x and y directions, respectively. The resulting interpolation functions are represented in Fig. 10.

Using these interpolation functions combined to a probabilistic model for the normalized displacements β_j, several realizations for the filter outputs can be constructed. In order to verify the interpolation and, thus the essential hypothesis used in this section, the filter outputs obtained in the previous section were reconstructed using (6). Figure 11 shows the average interpolation errors, compared to nominal values, of the first and second modal filter outputs.

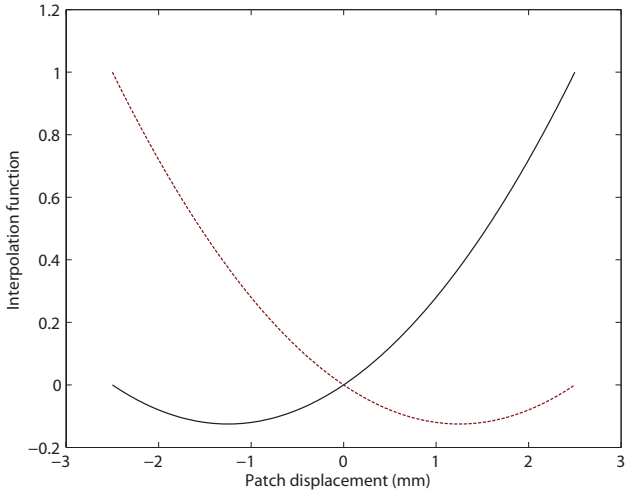

FIG. 10: Interpolation functions $0.5\beta_j(\beta_j + 1)$ and $0.5\beta_j(\beta_j - 1)$ used to construct the response surfaces.

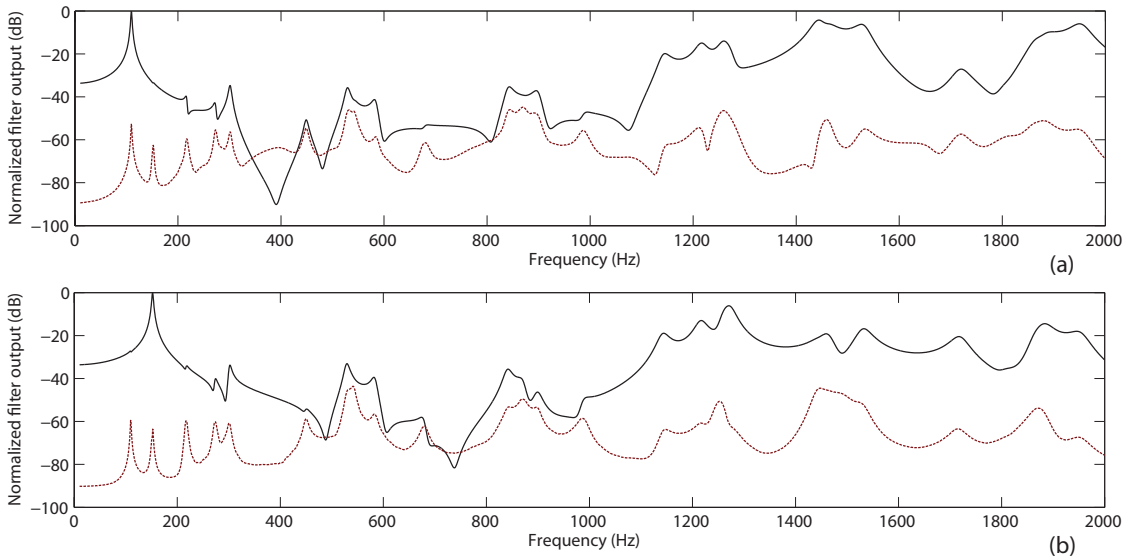

FIG. 11: Nominal (solid) and average interpolation error (dashed) values for normalized modal filter outputs; (a) first mode, (b) second mode.

These results validate the main hypothesis and, thus, the patches can be displaced individually without significant misrepresentation of the corresponding effect on the filter outputs.

Therefore, an analysis of the effect of positioning uncertainties on the modal filters outputs was performed by varying the 24 normalized displacements β_j (one displacement in x direction and one displacement in y direction for each of the 12 piezoelectric patches). A Gaussian probability density function is assumed for each normalized displacement β_j, with zero mean and $\sigma_\beta = 1/3$ standard deviation. This means that 99.73% of displacements should be smaller than one mesh step (that is 2.5 mm). Then,

$$p(\beta_j) = \frac{1}{\sqrt{2\pi}\sigma_\beta} \exp\left\{-\frac{\beta_j^2}{2\sigma_\beta^2}\right\}. \tag{7}$$

Based on these assumptions, N random realizations were generated for each normalized displacement with MATLAB function *normrnd* and, then, combined to evaluate N random realizations of the filter output frequency response function $\mathbf{G}_{int}$, according to (6). In the analysis presented in this work, $N = 3000$ Monte Carlo simulations were performed. The convergence of the Monte Carlo simulation was evaluated using

$$conv(N) = \frac{1}{N}\sum_{i=1}^{N} \|\mathbf{G}_{int}(\theta_i) - \mathbf{G}_M\|^2, \tag{8}$$

where $\mathbf{G}_M$ is the mean value of the filter output frequency response function. Figure 12 shows the mean-square convergence analysis. It is possible to observe that 500 simulations are enough to assure convergence. Despite that, the statistical analyses presented in the following sections consider all $N = 3000$ simulations performed.

Statistical analyses of the first and second modal filter output frequency response functions were performed using the percentiles to evaluate their mean and 95% confidence intervals (Fig. 13). As expected, the confidence intervals shown in Fig. 13 are smaller than the ones presented in the previous section (Figs. 5 and 6) since the present analysis allows smaller disturbances and accounts for a more realistic probability distribution of the perturbations. From the present analysis, the maximum filtering errors (within the filtering region up to 1000 Hz), considering the upper limit of the confidence intervals for the first and second modal filters, should be 5% (–25 dB) and 7% (–24 dB), respectively. Considering the mean filter outputs, the maximum filter output errors should be 2% (–34 dB) and 3% (–30 dB), respectively.

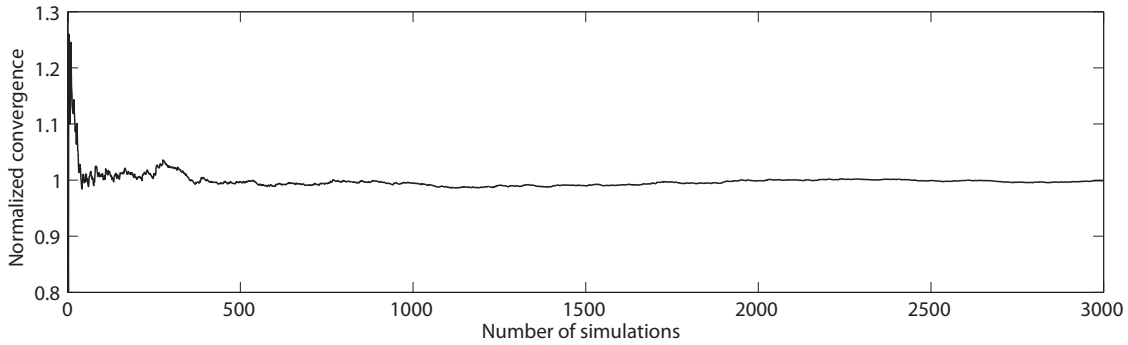

FIG. 12: Mean square convergence of Monte Carlo simulation.

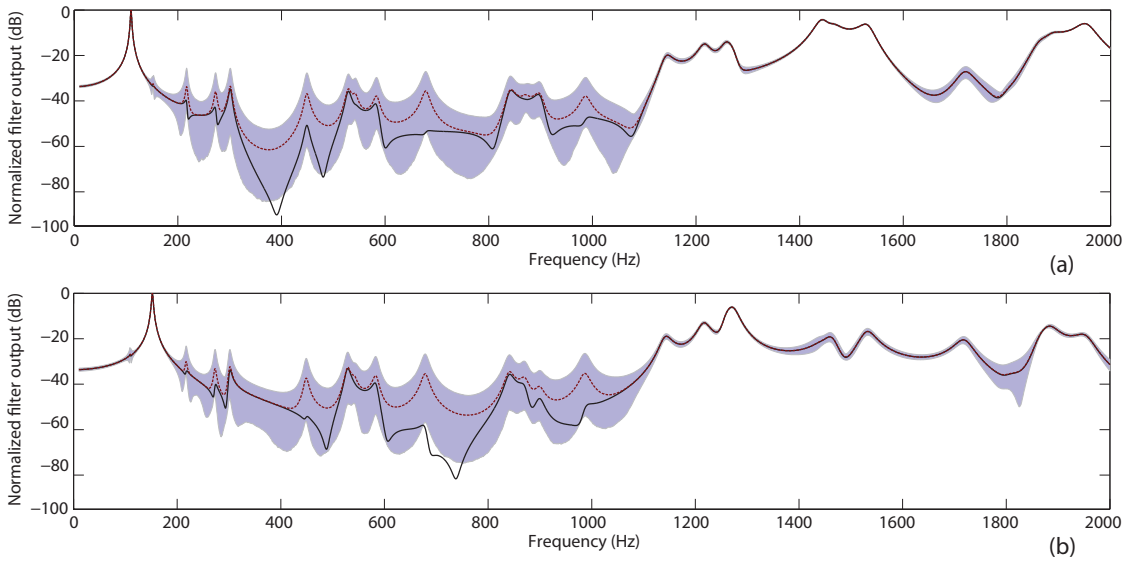

FIG. 13: Mean (dashed) and 95% confidence interval (filled) of normalized first (a) and second (b) filters outputs compared to nominal values (solid).

5. ANALYSIS OF WEIGHTING COEFFICIENTS UNCERTAINTIES

This section presents preliminary results of modal filters experimental implementation using optimal sensor array spatial distributions and its use for the analysis of the effect of weighting coefficients uncertainties on the modal filters effectiveness.

5.1 Experimental Implementation of Modal Filters

Experimental tests were designed to validate the proposed methodology for designing discrete modal filters using QR decomposition of FRF matrices, on one hand, and the optimal spatial distribution of 12 sensors obtained from numerical optimization, on the other hand. To this end, 12 transversely poled PIC151 piezoceramic patches (PI Ceramic) were bonded to one surface of a rectangular aluminum plate using an epoxy-based glue (Araldite) cured at 60°C. The 12 piezoceramic patches are identical, with dimensions $25\times25\times0.5$ mm. Small copper electrode layers were bonded on the top and bottom surfaces of each piezoceramic patch to enable independent measurement of the electric voltages induced on each patch.

The experimental setup considered for the validation of the modal filters performance predicted by the numerical analysis presented in [15] is presented in Fig. 14. An impact hammer (PCB model 086C03) was considered as the single force excitation applied at the upper-right corner of the rectangular plate, for the evaluation of the FRF measured by each one of the piezoelectric patches, used for the evaluation of the weighting coefficients, and also for the evaluation of the filtered FRF measured by the modal filter. A spectral analyzer (LMS SCADAS Mobile running on LMS Test.Lab software) was used for the acquisition of the voltage outputs at each piezoceramic patch and the force input measured at the impact hammer and for the evaluation of the FRF between them.

Then, the optimal weighting coefficients vector α_j for a modal filter designed to isolate the response of the jth vibration mode is evaluated using the QR decomposition of the experimental FRF measured by the 12 piezoelectric patches according to (5). The practical implementation of the weighted sum is obtained using the electric circuit shown in Fig. 15, composed of one voltage divider for each sensor and a summing amplifier to sum the weighted sensor signals. For that, the real part of the weighting coefficients, normalized to the maximum weight of 0.35 allowed by the designed voltage divider circuit, is evaluated and implemented in the weighted sum circuit board by adjusting the potentiometers. In this preliminary setup, a digital weighted sum was considered alternatively for some piezoelectric patches and when the weighting coefficients were too small and, thus, difficult to implement using the voltage divider circuit. In this case, the digital weighted sum was obtained with the help of a dSPACE control board (dSPACE DS1104).

After adjustment of the weighting coefficients, the filtered output signal, corresponding to the weighted sum of the 12 FRF measurements, is then fed back to the spectral analyzer. Hence, it should be possible to evaluate the FRF between the impact force and the weighted voltage sum. Since the evaluated optimal weighting coefficients are renormalized to the maximum weight of 0.35 allowed by the designed voltage divider circuit, the resulting filter outputs do not have unitary amplitude at target resonances. Hence, the filter outputs were renormalized by dividing the frequency response amplitude by its value at target resonance so that the amplitude at target resonance is unitary. Notice that there is no information loss, since the filtering performance is measured by the frequency response amplitudes relative to the one at target resonance. Figures 16–18 show the FRFs evaluated for a set of modal filters. These modal filters and, thus, their corresponding weighting coefficients vectors, were designed to isolate the responses of the first, second, and third vibration modes, respectively. Notice that the proposed spatial distribution of piezoelectric patches was designed to optimize the performance of the modal filters that isolate the response of the first and second vibration modes. Therefore, satisfactory results should only be expected for the first and second filters outputs. Indeed, both Figs. 16 and 17 present quite satisfactory results for the isolation of the first and second vibration modes responses, although it can be noticed that the modal filters using real (implemented) weighting coefficients (red curve) lead to higher error levels than the ones numerically evaluated using the ideal weighting coefficients (black curve). In particular for the first modal filter (Fig. 16), while the maximum amplitude in the frequency range of interest could be around 3% (at the fifth resonance) of the first resonance amplitude for ideal weighting

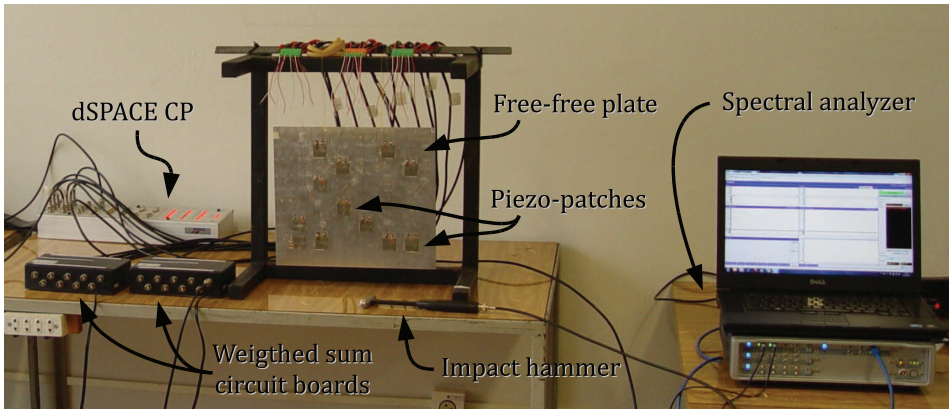

FIG. 14: Experimental setup: plate with 12 bonded piezoceramic patches.

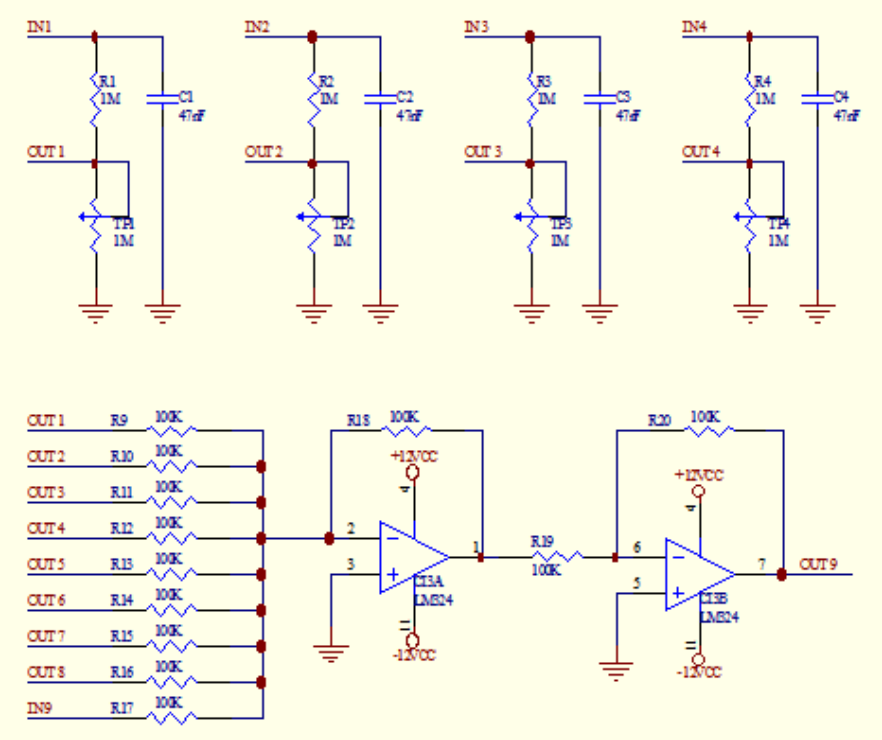

FIG. 15: Electric circuit designed for weighting and summing sensor signals.

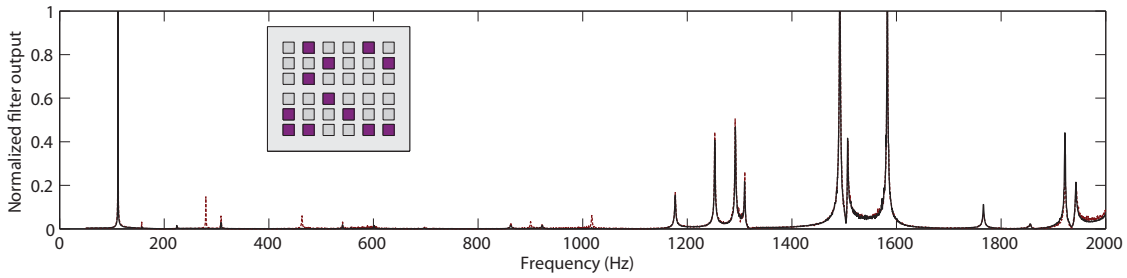

FIG. 16: Experimental normalized output of the modal filter designed for the isolation of the first vibration mode using ideal (black solid) and implemented (red dashed) weighting coefficients.

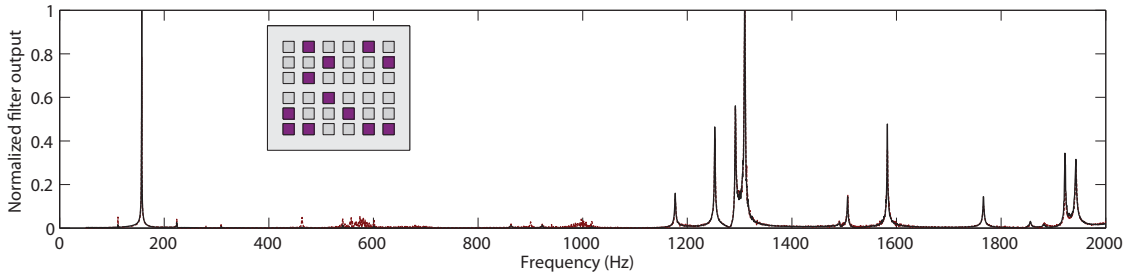

FIG. 17: Experimental normalized output of the modal filter designed for the isolation of the second vibration mode using ideal (black solid) and implemented (red dashed) weighting coefficients.

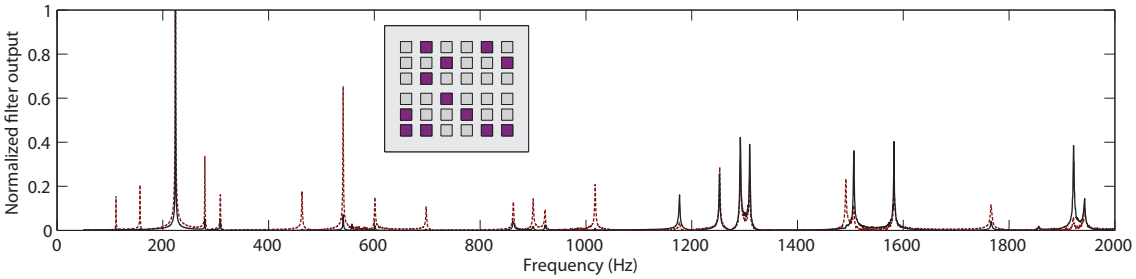

FIG. 18: Experimental normalized output of the modal filter designed for the isolation of the third vibration mode using ideal (black solid) and implemented (red dashed) weighting coefficients.

coefficients, the maximum amplitude of implemented modal filter reaches 15% of the first resonance amplitude (at the fourth resonance). For the second modal filter (Fig. 17), the maximum amplitude reaches 5% of the second resonance amplitude.

On the other hand, the output of the modal filter designed to isolate the response of the third vibration mode was not satisfactory (Fig. 18). This could be due to both inadequate design of the spatial distribution and implementation of weighting coefficients. However, since the maximum amplitude of the modal filter using ideal weighting coefficients is around 7% of the third resonance amplitude, it could be guessed that better performances should be obtained for this modal filter although the spatial distribution was not designed with that objective.

Another interesting result is obtained by combining the first and second modal filters to design a modal filter that isolates simultaneously the responses of the first and second vibration modes. This can be obtained using the sum of the corresponding weighting coefficients vectors. The resulting weighting coefficients vector was rescaled between 0 and 0.35 and implemented in the weighted sum circuit board. The output of this modal filter can be observed in Fig. 19. The filtering quality is satisfactory with maximum amplitude around 8% of the second resonance amplitude (while the ideal one should be around 3%).

5.2 Uncertainty Quantification Using Experimental/Numerical Analysis

From the observations of the previous section, it seems that the difficulty in implementing the weighting coefficients with the weighted sum circuit board is the main reason responsible for the differences between the ideal and real filter outputs. Therefore, this section presents an approach for analyzing the effect of random uncertainties in the weighting coefficients on the filters outputs. To build a stochastic model for the weighting coefficients, a Gaussian probability density function is assumed for each weighting coefficient α_{jk} ($k = 1, \ldots, 12$), with mean values based on the optimal ones designed to isolate the jth vibration mode response, and standard deviations are estimated from experiments, such that

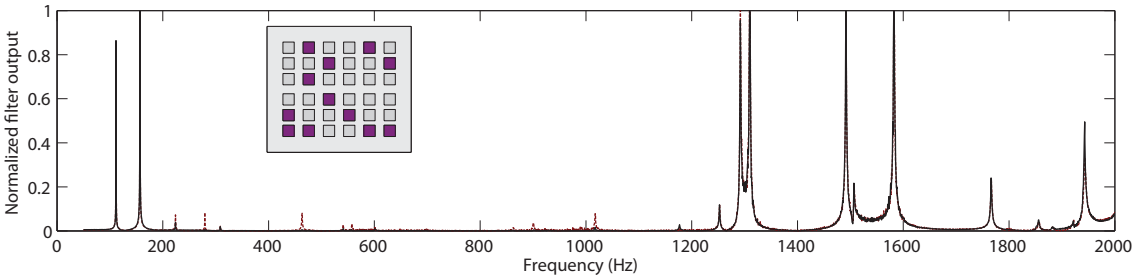

FIG. 19: Experimental normalized output of the modal filter designed for the isolation of the first and second vibration modes simultaneously using ideal (black solid) and implemented (red dashed) weighting coefficients.

$$p(\alpha_{jk}) = \frac{1}{\sqrt{2\pi}\sigma_\alpha} \exp\left\{-\frac{1}{2\sigma_\alpha^2}\left(\alpha_{jk} - \bar{\alpha}_{jk}\right)^2\right\}, \tag{9}$$

and where $\bar{\alpha}_{jk}$ are the real part of the weighting coefficients, normalized to the maximum weight of 0.35 allowed by the voltage divider circuit used for the measurements. σ_α is an estimation of the standard deviation based on experiments. Since the level of precision in the manual setup is much more dependent on the sensitivity of each potentiometer, the measurement technique for setup verification, and the user's experience, than on the nominal value of the weighting coefficient, the standard deviation σ_α was considered to be constant for all weighting coefficients. Based on laboratory experiments, the value of σ_α was set to 0.01.

Based on these assumptions, N random realizations were generated for each weighting coefficient with MATLAB function *normrnd* and, then, combined to form N random realizations of the vector of weighting coefficients $\alpha_j(\theta_i)$. Each realization $\alpha_j(\theta_i)$ was then used to evaluate a realization of the filter output $\tilde{\mathbf{G}}_j(\theta_i) = \mathbf{Y}\alpha_j(\theta_i)$, where $\mathbf{Y}$ are the experimental frequency response functions measured by the piezoelectric patches. The mean-square convergence analysis with respect to the independent realizations $\tilde{\mathbf{G}}_j(\theta_i)$ was carried out considering the function

$$conv(N) = \frac{1}{N}\sum_{i=1}^{N} \|\tilde{\mathbf{G}}_j(\theta_i) - \tilde{\mathbf{G}}_j^N\|^2, \tag{10}$$

where N is the number of simulations, or the number of sets of weighting coefficients considered, and $\tilde{\mathbf{G}}_j^N$ is the response calculated using the corresponding nominal (ideal) model. It was observed that around 2000 simulations were enough to assure convergence. Despite that, the statistical analyses presented in the following sections consider all $N = 4000$ simulations performed.

The statistical analyses of FRF amplitudes were performed using their 4000 realizations at each frequency to calculate the corresponding mean values and 95% confidence intervals. The 95% confidence intervals were evaluated using the 2.5% and 97.5% percentiles of the realizations of FRF amplitudes at each frequency. More details on the stochastic modeling methodology used here can be found in [17–19].

The experimental (real) normalized outputs of the modal filters compared to ideal ones and their 95% confidence intervals are presented in Figs. 20–22. They correspond, respectively, to the modal filters designed to isolate the first, second, third, and first and second vibration modes simultaneously. From Figs. 20 and 21, it could be concluded that the variability of the weighting coefficients almost completely explains the experimental filter outputs (since they are inside the confidence intervals). A similar result is observed for the modal filter designed to isolate the first and second vibration modes response simultaneously (Fig. 22). On the other hand, this is not true for the modal filter designed to isolate the response of the third vibration mode, for which the output is presented in Fig. 23. In this case, the filter output does not coincide with the 95% confidence interval and, thus, the difference between real and ideal modal filter output could be mainly due to another reason (besides weighting coefficients variability).

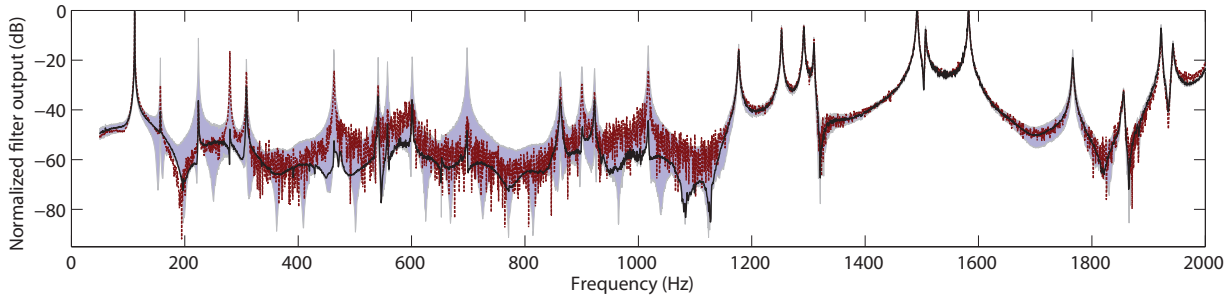

FIG. 20: Experimental normalized output of the first mode modal filter using ideal (solid) and implemented (dashed) weighting coefficients and its confidence interval for uncertain weighting coefficients with $\sigma_\alpha = 0.01$ (filled).

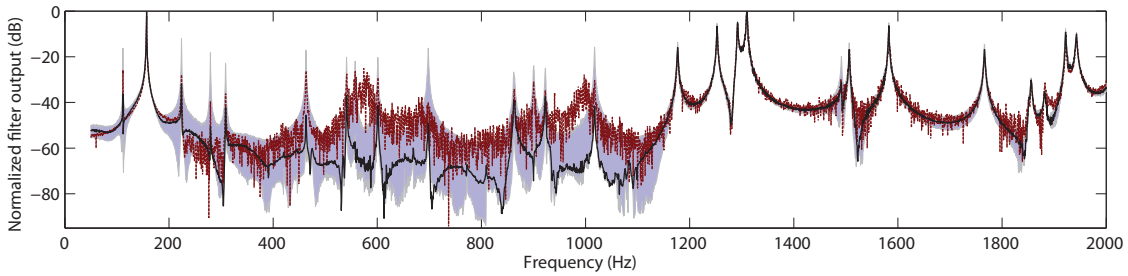

FIG. 21: Experimental normalized output of the second mode modal filter using ideal (solid) and implemented (dashed) weighting coefficients and its confidence interval for uncertain weighting coefficients with $\sigma_\alpha = 0.01$ (filled).

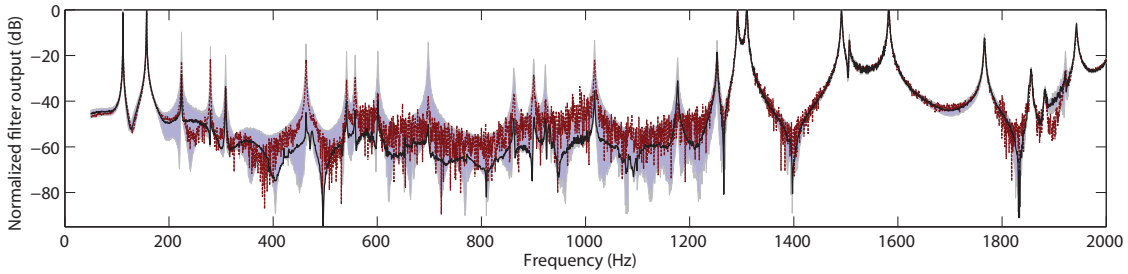

FIG. 22: Experimental normalized output of the first and second modes modal filter using ideal (solid) and implemented (dashed) weighting coefficients and its confidence interval for uncertain weighting coefficients with $\sigma_\alpha = 0.01$ (filled).

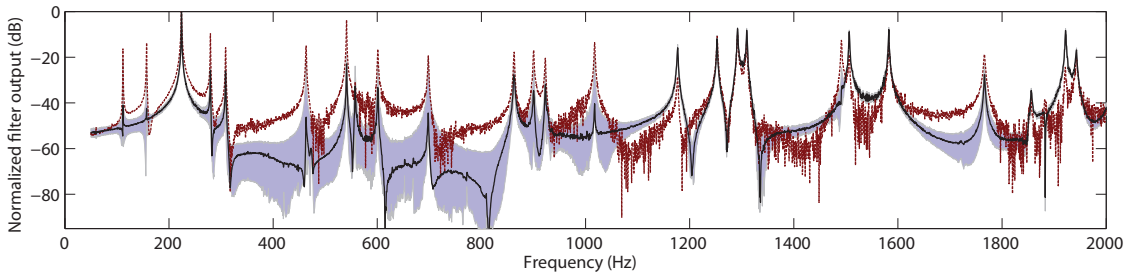

FIG. 23: Experimental normalized output of the third mode modal filter using ideal (solid) and implemented (dashed) weighting coefficients and the confidence interval for uncertain weighting coefficients with $\sigma_\alpha = 0.01$ (filled).

6. CONCLUSIONS AND FUTURE WORKS

This work has presented some recent numerical and experimental results about the effect of uncertainties of the sensor array spatial distribution and of the weighting coefficients on the effectiveness of a series of modal filters. For the sensors positioning uncertainties, two sampling-based sensitivity analyses were performed. In the first one, the Latin hypercube sampling technique was used to reduce the number of samples and alleviate the computational cost of analyzing multiple spatial distributions. It was shown that for perturbation displacements smaller than 2.5 mm, the filtering error should be smaller than approximately 10%. In the second one, a response surface method was used to evaluate the effect of smaller disturbances. It was shown that filtering errors below 25 dB for the first and second modal filters, respectively, could be expected. For the weighting coefficients uncertainties, a numerical/experimental analysis was performed using experimental FRFs measured by the piezoelectric patches and uncertain weighting coefficients,

which were varied in a Monte Carlo simulation according to a Gaussian probability density function. It was shown that the variability considered for the weighting coefficients may increase the filtering errors by 10–20 dB. However, these results also show that although modal filters can be sensitive to both positioning and weighting coefficients uncertainties, the chosen array of piezoceramic sensors still yields high quality modal filters up to 1100 Hz. The main contribution of the present work is to provide an original quantitative analysis of the effect of uncertainties of sensors positioning and weighting coefficients on the performance of spatial modal filters. The results show that the filtering performance is generally more sensitive to uncertainties/variations of weighting coefficients than those of sensors positioning. This means that special care should be taken when designing the weighted-sum circuit or similar.

ACKNOWLEDGMENTS

The authors acknowledge the support of the MCT/CNPq/FAPEMIG National Institute of Science and Technology on Smart Structures in Engineering, grant no. 574001/2008-5, and the State of São Paulo Research Foundation (FAPESP), grant no. 10/02198-4.

REFERENCES

1. Sunar, M. and Rao, S., Recent advances in sensing and control of flexible structures via piezoelectric materials technology, *Appl. Mech. Rev.*, 52(1):1–16, 1999.
2. Ahmadian, M. and Deguilio, A., Recent advances in the use of piezoceramics for vibration suppression, *Shock Vibration Dig.*, 33(1):15–22, 2001.
3. Reza Moheimani, S., A survey of recent innovations in vibration damping and control using shunted piezoelectric transducers, *IEEE Tran. Control Syst. Technol.*, 11(4):482–494, 2003.
4. Park, G., Sohn, H., Farrar, C. R., and Inman, D. J., Overview of piezoelectric impedance-based health monitoring and path forward, *Shock Vibration Dig.*, 35(6):451–463, 2003.
5. Giurgiutiu, V. and Cuc, A., Embedded non-destructive evaluation for structural health monitoring, damage detection, and failure prevention, *Shock Vibration Dig.*, 37(2):83–105, 2005.
6. Sodano, H. A., Inman, D. J., and Park, G., A review of power harvesting from vibration using piezoelectric materials, *Shock Vibration Dig.*, 36(3):197–205, 2004.
7. Meirovitch, L. and Baruh, H., Control of self-adjoint distributed-parameter systems, *AIAA J. Guidance, Control and Dynamics*, 5(1):60–66, 1982.
8. Lee, C. and Moon, F., Modal sensors/actuators, *J. Appl. Mech.*, 57(2):434–441, 1990.
9. Fripp, M. and Atalla, M., Review of modal sensing and actuation techniques, *Shock Vibration Dig.*, 33(1):3–14, 2001.
10. Preumont, A., François, A., De Man, P., and Piefort, V., Spatial filters in structural control, *J. Sound Vibration*, 265(1):61–79, 2003.
11. Friswell, M., On the design of modal actuators and sensors, *J. Sound Vibration*, 241(3):361–372, 2001.
12. Chen, C.-Q. and Shen, Y.-P., Optimal control of active structures with piezoelectric modal sensors and actuators, *Smart Mater. Struct.*, 6(4):403–409, 1997.
13. Tanaka, N. and Sanada, T., Modal control of a rectangular plate using smart sensors and smart actuators, *Smart Mater. Struct.*, 16(1):36–46, 2007.
14. Shelley, S., Investigation of discrete modal filters for structural dynamic applications, Ph.D. Thesis, University of Cincinnati, 1991.
15. Pagani, Jr., C. and Trindade, M., Optimization of modal filters based on arrays of piezoelectric sensors, *Smart Mater. Struct.*, 18(9):095046, 2009.
16. Helton, J., Johnson, J., Sallaberryc, C., and Storlie, C., Survey of sampling-based methods for uncertainty and sensitivity analysis, *Reliability Eng. Syst. Safety*, 91:1175–1209, 2006.
17. Cataldo, E., Soize, C., Sampaio, R., and Desceliers, C., Probabilistic modeling of a nonlinear dynamical system used for producing voice, *Comput. Mech.*, 43(2):265–275, 2009.

18. Soize, C., Maximum entropy approach for modeling random uncertainties in transient elastodynamics, *J. Acoust. Soc. Am.*, 109:1979–1996, 2001.
19. Santos, H. and Trindade, M., Structural vibration control using extension and shear active-passive piezoelectric networks including sensitivity to electrical uncertainties, *J. Braz. Soc. Mech. Sci. Eng.*, 33(3):287–301, 2011.